Semi-Infinite Hydraulic Fracture Driven by a Sequence of Power-Law Fluids

Alena Bessmertnykh, Ph.D.[1]; Egor Dontsov, Ph.D.[2]; and Roberto Ballarini, Ph.D., P.E., Dist.M.ASCE[3]

Abstract: Hydraulic fracturing technology most often involves multiple fluids with different properties to achieve desired treatments. This study examines the effects of multiple sequential fluids on the stress, strain, and deformation fields in the near-tip region of a semi-infinite fracture. It is assumed that the immiscible displacement of multiple power-law fluids is separated by stable boundaries. The fracture opening of a steadily propagating hydraulic fracture is computed by solving the elasticity and lubrication equations. The numerical solution correctly captures the well-known asymptotic behavior at the crack tip for multiple fluids. Specifically, the multiple-fluids solution asymptotically approaches the solution for the first fluid in the immediate vicinity of the tip and approaches the solution corresponding to the last fluid far from the tip. In the transition region, the behavior depends on the presence of additional fluids and the locations of their respective boundaries. Illustrative results for multiple fluids with different properties and boundary locations are included. **DOI: 10.1061/(ASCE)EM.1943-7889.0001958.**

Author keywords: Hydraulic fracture; Tip asymptotics; Linear elastic rock; Power-law fluid; Multiple fluids.

Introduction

Hydraulic fracturing is widely used worldwide to increase production of hydrocarbons from unconventional reservoirs (Economides and Nolte 2000; Belyadi et al. 2016). In this process, highly pressurized fluids are injected into the underground through a wellbore to create cracks within the rock formation, which serve as conductive paths for hydrocarbons to flow into the wellbore and, in turn, to the surface. Depending on the completion design, different types of fracturing fluids can be used at different stages of the process, e.g., low-viscosity slick water, more viscous linear or cross-linked gels, multiphase emulsions, or polymer or foam solutions, just to name a few (Barbati et al. 2016; Montgomery 2013). The additives introduced into the base fluids lead to desired fluid properties and often make the behavior of the mixtures non-Newtonian. The nonlinear shear stress of such fluids is often modeled using power-law rheological models, but other types of models have also been used.

Modeling sequential injection of multiple fluids into a fracture is a challenging problem because the presence of interfaces between fluids may involve complex phenomena such as hydrodynamic instabilities in both miscible and immiscible fluids (Truzzolillo and Cipelletti 2017). In addition, when one fluid is displaced by another fluid, the effects of gravity (if there is a contrast in specific gravities) and viscous fingering (if there is a contrast in viscosities) can be significant. It is known that Saffman-Taylor instabilities or viscous fingering (Saffman and Taylor 1958) may occur when a higher-viscosity fluid is displaced by a lower-viscosity fluid. The instabilities are dictated, among other factors, by the constitutive equations of the fluids and capillary forces.

A stable fluid displacement is considered favorable for certain oil and gas applications. In practice, one of the most common scenarios involves the injection of a lower-viscosity fluid ahead of a higher-viscosity fluid (Barbati et al. 2016) that includes granular additives (proppant) of larger size. In this paper, it is assumed that the fluids do no mix and are separated by a discernible interface originating from the interfacial tension. This is a common assumption that was used, for instance, by Lakhtychkin et al. (2011, 2012) to account for multiple fluids within an elliptical fracture. This paper uses the latter assumption to study the effect of multiple fluids on the near-front behavior of a hydraulic fracture.

In hydraulic fracturing, fluid loss through porous rock surrounding the fracture is conventionally modeled using Carter's leak-off model (Economides and Nolte 2000; Adachi 2001), which accounts for leak-off via an additional sink term in the mass-balance equation. This circumvents the need to solve a multiphase diffusion problem in the reservoir, which could significantly complicate the overall problem formulation and increase its computational cost. Carter's leak-off model considers the presence of three filtration mechanisms associated, respectively, with filter cake, invaded zone, and reservoir diffusion. The fluid filtration is characterized by a lumped leak-off coefficient C_L encompassing the total fluid loss via these three possibilities, and the model is characterized by the inverse square-root time dependence of the leak-off flux.

Often, fracturing fluid consists of a mixture of Newtonian fluid and polymers, which results in non-Newtonian rheology that is readily modeled with a power-law model. During leak-off, polymers tend to form a filter cake while the base Newtonian fluid leaks into the reservoir, creating the invaded zone. Outside of the invaded zone occupied by the base fracturing fluid, there is reservoir fluid, whose pressure is also disturbed by leak-off; this comprises the last mechanism for fluid leak-off resistance. The carrier fluid itself can be non-Newtonian. In this case, the filter cake building mechanism becomes more complex and the leak-off time dependence may deviate from the inverse square root behavior featured in Carter's model. Such situations, however, are not considered in this paper, and the fluid loss mechanism is modeled using conventional Carter's

[1]Research Assistant, Dept. of Civil and Environmental Engineering, Univ. of Houston, Houston, TX 77204 (corresponding author). ORCID: https://orcid.org/0000-0001-5087-3940. Email: abessmertnykh@uh.edu

[2]Chief Scientist, ResFrac Corporation, 555 Bryant St., Palo Alto, CA 94301. ORCID: https://orcid.org/0000-0002-0437-4910

[3]Thomas and Laura Hsu Professor and Department Chair, Dept. of Civil and Environmental Engineering, Univ. of Houston, Houston, TX 77204.

Note. This manuscript was submitted on October 18, 2020; approved on March 15, 2021; published online on July 24, 2021. Discussion period open until December 24, 2021; separate discussions must be submitted for individual papers. This paper is part of the ***Journal of Engineering Mechanics***, © ASCE, ISSN 0733-9399.

leak-off model, which has also been previously used in the context of the semi-infinite fracture geometry for power-law fluids by Dontsov and Kresse (2018).

Also, all fluids are assumed to have the same leak-off coefficient for simplicity. Although it is technically possible to assign various coefficients to different fluids, it would probably not provide a more accurate description of the process. For instance, if one fluid is followed by another, then the second fluid filtrates through the filter cake formed by the first fluid. And then, there can be two types of filter cakes one over another. It is unlikely that Carter's model will be very accurate in this case. Moreover, given the complexity of physical mechanisms involved in the calculation of leak-off, it is difficult to precisely estimate the value of the leak-off coefficient. In practice, the effective Carter's coefficient is estimated through field testing, and doing so for each fluid may not be practical. Due to the aforementioned reasons, the analysis is restricted to a single value of the leak-off coefficient for all fluids.

The near-front region is modeled as a semi-infinite hydraulic fracture propagating under plane-strain conditions. It is well-known that the behavior near the front of fluid-driven cracks has a multiscale nature (Detournay 2016): multiple regions exist whose behavior is dictated by different physical parameters and processes such as rock toughness, fluid leak-off from the fracture into the adjacent rock formation, and fluid viscosity. The asymptotics corresponding to toughness, leak-off, and viscosity dominated solutions for power-law fluids were obtained by Rice (1968), Lenoach (1995), and Desroches et al. (1994). The multiscale asymptotic solution that captures all the phenomena for Newtonian fluids was obtained by Garagash et al. (2011), and its fast approximation that is particularly relevant for applications was constructed by Dontsov and Peirce (2015b). The general solution for power-law fluids, which is of special interest for this paper, was obtained by Gomez (2016) and Dontsov and Kresse (2018).

Near-tip asymptotic solutions are used in hydraulic fracture (HF) simulations in various ways. First, the near-tip logic provided by asymptotic solutions can be effectively used to accurately track the location of the fracture front. Second, multiscale asymptotic solutions can be used to rapidly estimate fracture dimensions. The latter idea was initially proposed for penny-shaped and plane-strain hydraulic fractures by Dontsov (2016, 2017) and then extended to an elliptical hydraulic fracture in a transversely isotropic material by Bessmertnykh and Dontsov (2018), Dontsov (2019), and Moukhtari et al. (2020). It has also been used to construct the ultrafast hydraulic fracturing simulator to rapidly simulate multiple fractures by Dontsov et al. (2019). The application of the near-tip logic as a propagation condition was implemented in the displacement discontinuity method (Dontsov and Peirce 2017) and finite-element method (Gordeliy and Peirce 2013; Peirce 2016) using the implicit level set algorithm initially proposed by Peirce and Detournay (2008). A comparison of using the asymptotics as near-tip logic with other approaches has been given by Lecampion et al. (2013).

This paper assumes the simultaneous presence of multiple fluids within a semi-infinite fracture, which represents the near-tip model for a finite fracture with multiple fluids. Application of the multifluid near-tip asymptotics may be invoked depending on the mesh used in the hydraulic fracturing simulator, as well as the injection schedule. For high-fidelity models with fine meshes, the tip element often includes only one kind of fluid, and applying the lumped multifluid asymptote in the tip element is not necessary. However, if the number of elements per fracture is small, which is often desired in practice to improve computational performance, the tip element can extend further inside the fracture and cover the region with multiple fluids. In the latter case, implementing the multifluid asymptotic solution significantly improves the accuracy of the model.

For example, there is a class of existing ultrafast hydraulic fracturing simulators that aim to rapidly estimate fracture geometry for the purpose of sensitivity analysis (Dontsov et al. 2019; Peshcherenko and Chuprakov 2021). Such models keep only the dominant mechanisms to describe the behavior of the hydraulic fracture and restrict the shape to a rectangular (Peshcherenko and Chuprakov 2021) or an elliptical geometry with using virtually a single element per fracture length (Dontsov et al. 2019). The primary focus of the present work is to improve the accuracy of the aforementioned ultrafast hydraulic fracturing simulators (e.g., Dontsov et al. 2019), by enabling them to account for the presence of multiple fluids. However, this fundamental study may also be beneficial for other applications.

The near-tip asymptotic solution developed in this study has been implemented in the previously mentioned ultrafast HF simulator (Dontsov et al. 2019). The full simulator tracks the interfaces between fluids using the Lagrangian approach based on volume balance and the specified fluid injection schedule. A similar idea was implemented by Dontsov and Peirce (2015a) to keep track of proppant placement in a hydraulic fracture and its time evolution. Consequently, locations of the fluid interfaces are calculated in the HF simulator for the full fracture at each time moment. These are instantaneous locations that can evolve in time, e.g., due to a diverging flow or leak-off. In addition, because the Lagrangian approach is used, these boundaries are not collocated with the fracture mesh, which results in the possibility of having multiple fluids and multiple interfaces within a single fracture element. Therefore, the boundaries between fluids are treated as input parameters for the problem of a semi-infinite fracture under consideration. In addition, their evolution in time is assumed to be relatively slow, so that the effect of their dynamics is neglected within the semi-infinite fracture model.

This paper solves the problem of a semi-infinite fracture driven by multiple sequential power-law fluids under the assumption of stable immiscible displacement. The formulation is a significant extension of a similar approach developed for a single power-law fluid (Gomez 2016; Dontsov and Kresse 2018). Section "Problem Statement" formulates the problem of the idealized geometry of a hydraulic fracture containing multiple fluids. Section "Governing Equations" presents the elasticity and lubrication equations that govern the problem, and their scaled version is given in the section "Scaled Form of the Governing Equations." Limiting asymptotic solutions are provided in the section "Asymptotic Solutions." Section "Numerical Results" presents and discusses illustrative numerical results, and the section "Summary" summarizes the findings.

Problem Statement

This study considers a semi-infinite crack that represents the near-tip region of a HF within which N fluids are pumped sequentially, as depicted in Fig. 1. The HF is propagating steadily with velocity V in the direction of a moving coordinate system x, which represents the distance from the fracture tip; $w(x)$ is the crack opening displacement (width), whose solution is of interest. The fluids are distinguished using different shades, and the parameters of the ith fluid, n_i, k_i, refer to their power-law model

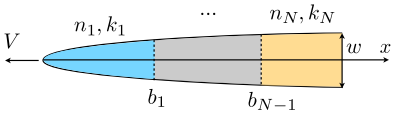

Fig. 1. Scheme of a semi-infinite hydraulic fracture with N power-law fluids.

$$\tau = k\dot{\gamma}^n, \qquad \dot{\gamma} = \frac{\partial v}{\partial y} \tag{1}$$

where τ = shear stress; v = fluid velocity; k = consistency index; and n = behavioral index. The location of the interfaces between ith and $(i+1)$th fluid, b_i, is prescribed and assumed to be fixed in the moving coordinate system. This assumption is valid if the displacement of the immiscible fluids is stable and the transitional zone between them is small. Strictly speaking, the assumption of zero fluid loss (or leak-off) is also necessary to preserve the location of fluid interfaces. However, the examples with leak-off are still considered in this paper for completeness, keeping in mind that the dynamics of fluid interfaces is neglected.

To justify the assumption of stable interfaces between fluids, consider two distinct fluids flowing sequentially in a channel. The shape and stability of the interface between the fluids are determined by the competition between viscous forces and capillary forces caused by surface tension. The channel flow of a viscous fluid has a nonuniform velocity profile that leads to distortion of the interface between fluids. In contrast, the forces of surface tension act to minimize the surface area of the interface. The interface is stable or retains its shape when the capillary forces are able to compensate the distortion of the interface caused by viscous forces (Al-Housseiny et al. 2012; Woods and Mingotti 2016). The capillary pressure can be estimated as follows:

$$p_c = \frac{2(\sigma_1 - \sigma_2)}{R} \tag{2}$$

where σ_i = surface tension of the ith fluid; and R = radius of curvature of the interface between fluids. The viscous forces for the considered problem can be estimated using Eq. (1) where $\dot{\gamma} \sim V/w$ with V varying from $\sim 10^{-2}$ to 10^{-1} m/s and $w \sim 1$ mm. Consider two fluids with the following properties: surface tension $\sigma_1 = 80$ mN/m and $\sigma_2 = 60$ mN/m, flow indices $n_1 = 1$ and $n_2 = 1$, and consistency indices $k_1 = 3\,\text{mPa}\cdot\text{s}$ and $k_2 = 40\,\text{mPa}\cdot\text{s}$. By equating viscous [Eq. (1)] and capillary [Eq. (2)] forces, the critical radius of curvature for the interface can be estimated as $R \sim 1$–10 cm. At the same time, the fracture opening near the fracture tip w is typically on the order of several millimeters, which is less than the estimated radius of curvature, i.e., as follows:

$$R \gg O(w), \quad \text{where } R \approx \frac{2(\sigma_1 - \sigma_2)}{k\dot{\gamma}^n} \tag{3}$$

In this case, the interface is kept stable by the capillary forces. Otherwise, if Eq. (3) is not satisfied, the fluid interface may become unstable, which is not considered in this study. When the fluid displacement is stable ($R \sim 1$–10 cm), the capillary pressure jump over the fluid interface [Eq. (2)] is less than ~ 4 Pa. Generally, capillary pressure (order of Pa) is negligibly small compared with the typical net pressure values in hydraulic fracturing (order of MPa). Another possible way to estimate this is to consider the change of the stress intensity factor caused by the capillary pressure, $\Delta K_I \propto p_c\sqrt{b}$ (Rice 1968), where b is the distance from the tip to the interface. Given that the upper bound for b can be up to 100 m, the additional stress intensity factor is bounded by $50\ \text{Pa}\cdot\text{m}^{1/2}$, which is much less than typical rock toughness of $1\ \text{MPa}\cdot\text{m}^{1/2}$ (Economides and Nolte 2000). Therefore, the contribution of capillary pressure to the stress intensity factor can be neglected.

Governing Equations

The system of governing equations consists of the linear elasticity equation for the rock formation, the lubrication equation describing the fluids, and the fracture propagation criterion; the coupled system is solved for the crack width $w(x)$. The equations are rewritten by scaling the material properties as follows:

$$E' = \frac{E}{1-\nu^2}, \qquad K' = 4\left(\frac{2}{\pi}\right)^{1/2} K_{Ic}, \qquad C' = 2C_L,$$
$$M_i' = \frac{2^{n_i+1}(2n_i+1)^{n_i}}{n_i^{n_i}} k_i \tag{4}$$

where ν = Poisson's ratio; E = Young's modulus; K_{Ic} = fracture toughness of the rock; C_L = leak-off coefficient; and n_i and k_i = rheological parameters of the ith power-law fluid [Eq. (1)].

Elasticity Equation and Fracture Propagation Condition

The relation between the pressure $p(x)$ and the crack opening width $w(x)$ for the semi-infinite fracture is written as the integral equation

$$p(x) = \frac{E'}{4\pi}\int_0^\infty \frac{\mathrm{d}w}{\mathrm{d}s}\frac{\mathrm{d}s}{x-s} \tag{5}$$

To avoid the singularity of the fluid pressure at the fracture tip, the inverted form of the elasticity equation is used (Spence et al. 1987; Roper and Lister 2007; Dontsov and Peirce 2015b)

$$w(x) = \frac{K'}{E'}x^{1/2} - \frac{4}{\pi E'}\int_0^\infty F(x,s)\frac{\mathrm{d}p}{\mathrm{d}s}\mathrm{d}s \tag{6}$$

with the kernel

$$F(x,s) = (s-x)\ln\left|\frac{x^{1/2}+s^{1/2}}{x^{1/2}-s^{1/2}}\right| - 2x^{1/2}s^{1/2} \tag{7}$$

The fracture propagation criterion $K_I = K_{Ic}$ results in the following asymptotic behavior for the crack opening near the fracture tip:

$$w = \frac{K'}{E'}x^{1/2}, \qquad x \to 0 \tag{8}$$

Lubrication Equation

To formulate the lubrication equation, the following assumptions are made:

- Fluid displacement is immiscible, and any instabilities at the interfaces between fluids are neglected.
- The width of the transition zone between the fluids is negligibly small.
- Dispersion effects associated with the presence of multiple fluids are neglected.
- Gravity is neglected.
- All fluids have equal Carter's leak-off coefficient.

Define ϕ_i as the volume fraction of the ith fluid. The volume balance equation for each fluid can be written

$$\frac{\partial \phi_i w}{\partial t} + \frac{\partial \phi_i q}{\partial \hat{x}} + \phi_i q_L = 0 \tag{9}$$

where $\hat{x}$ = absolute spatial coordinate whose direction is opposite to x shown in Fig. 1; and q = total flux inside the fracture. The flux of fluid leaking off to the rock formation obeys Carter's model (Carter 1957)

$$q_L = \frac{C'}{\sqrt{\tau(\hat{x})}} \tag{10}$$

where τ = time elapsed since the fluid reached point $\hat{x}$ for the first time.

In a coordinate system moving with a velocity V illustrated in Fig. 1, $x = Vt - \hat{x}$ and Eq. (9) with Eq. (10) is rewritten in the following form:

$$V\frac{\mathrm{d}w\phi_i}{\mathrm{d}x} - \frac{\mathrm{d}\phi_i q}{\mathrm{d}x} + \phi_i C'\sqrt{\frac{V}{x}} = 0 \tag{11}$$

which, after integration, gives the following expression for the total fluid flux:

$$q = Vw + 2C'\sqrt{Vx} \tag{12}$$

Alternatively, the total flux can be obtained by summing the contributions from all fluids with weights given by their volume fractions

$$q = \sum_{i=1}^{N} \phi_i q_i \tag{13}$$

Neglecting the transition zone between fluids, the interface between fluids is assumed to be flat and the volume fractions are given by

$$\phi_1 = (1 - H(x - b_1)), \qquad \phi_N = H(x - b_{N-1}) \tag{14}$$

for the first and the last fluids, and

$$\phi_i = H(x - b_{i-1}) - H(x - b_i), \qquad i = 2, \ldots, N-1 \tag{15}$$

for all intermediate fluids. The Heaviside function $H(\cdot)$ is used to define the presence of the ith fluid between boundaries b_{i-1} and b_i. In this case, the flux for each fluid, q_i, in a channel is given by the power-law rheological model [Eq. (1)]

$$|q_i| = \left(\frac{w^{2n_i+1}}{M'_i}\left|\frac{\partial p}{\partial x}\right|\right)^{1/n_i} \quad \text{at} \quad \phi_i = 1 \tag{16}$$

The pressure gradient for the particular ith fluid, which can be explicitly found by equating expressions for fluid flux [Eqs. (12) and (13)] using Eq. (16) at $\phi_i = 1$, reads

$$\left(\frac{\mathrm{d}p}{\mathrm{d}x}\right)_i = (Vw + 2C'V^{1/2}x^{1/2})^{n_i}\frac{M'_i}{w^{2n_i+1}} \quad \text{at} \quad \phi_i = 1 \tag{17}$$

The pressure gradient for multiple fluids undergoes discontinuous change on the boundaries between fluids

$$\begin{aligned}\frac{\mathrm{d}p}{\mathrm{d}x} = {} & \left(\frac{\mathrm{d}p}{\mathrm{d}x}\right)_1 (1 - H(x - b_1)) \\ & + \sum_{i=2}^{N-1}\left(\frac{\mathrm{d}p}{\mathrm{d}x}\right)_i (H(x - b_{i-1}) - H(x - b_i)) \\ & + \left(\frac{\mathrm{d}p}{\mathrm{d}x}\right)_N H(x - b_{N-1})\end{aligned} \tag{18}$$

whereas the pressure itself is continuous because the capillary pressure drop is neglected. After substitution of Eq. (18) into the elasticity Eq. (6) using Eq. (17), the final governing equation for fracture width can be written in the following form:

$$\begin{aligned}w(x) = {} & \frac{K'}{E'}x^{1/2} - \frac{4}{\pi E'}\int_0^\infty F(x,s)\Bigg((Vw + 2C'V^{1/2}x^{1/2})^{n_1} \\ & \times \frac{M'_1}{w^{2n_1+1}}(1 - H(x - b_1)) + \sum_{i=2}^{N-1}(Vw + 2C'V^{1/2}x^{1/2})^{n_i} \\ & \times \frac{M'_i}{w^{2n_i+1}}(H(x - b_{i-1}) - H(x - b_i)) \\ & + (Vw + 2C'V^{1/2}x^{1/2})^{n_N}\frac{M'_N}{w^{2n_N+1}}H(x - b_{N-1})\Bigg)\mathrm{d}s\end{aligned} \tag{19}$$

Scaled Form of the Governing Equations

The numerical calculations adapted a set of dimensionless quantities consistent with previous studies (Dontsov and Peirce 2015b; Dontsov and Kresse 2018; Bessmertnykh and Dontsov 2019)

$$\begin{aligned}&\tilde{w} = \frac{wE'}{K'x^{1/2}}, \qquad \tilde{x} = \left(\frac{x}{l}\right)^{1/2}, \qquad \tilde{s} = \left(\frac{s}{l}\right)^{1/2}, \qquad \chi = \frac{2C'E'}{V^{1/2}K'}, \\ &l = \left(\frac{K'^{n_w+2}}{M'_w V^{n_w}E'^{n_w+1}}\right)^{2/(2-n_w)}, \qquad l_i = \left(\frac{K'^{n_i+2}}{M'_i V^{n_i}E'^{n_i+1}}\right)^{2/(2-n_i)}, \\ &\xi_i = \frac{M'_i V^{n_i}E'^{(n_i+1)}}{K'^{n_i+2}l^{(n_i-2)/2}} = \left(\frac{l_i}{l}\right)^{(n_i-2)/2}, \qquad \tilde{b}_i = \left(\frac{b_i}{l}\right)^{1/2}\end{aligned} \tag{20}$$

where $\tilde{w}$ = scaled fracture opening; $\tilde{x}$ = distance from the fracture front; χ = leak-off coefficient; l = length scale introduced based on the parameters of water ($n_w = 1, k_w = 1\,\mathrm{mPa}\cdot\mathrm{s}$); l_i = length scale based on the parameters of the ith fluid; and $\tilde{b}_i$ = boundary between the ith and the $(i+1)$th fluids.

Unlike previous studies for a single fluid, the case of multiple fluids involves an additional dimensionless parameter ξ_i that characterizes distinct properties of fluids. The parameter ξ_i is written in terms of the length scales; for the fluids whose properties (n_i and k_i) are the same as for water, $l_i = l$ and $\xi_i = 1$. The length scale l can be chosen arbitrarily or can be based on the properties of one of the fluids. Here, l is defined based on the properties of water and used throughout the paper.

By using the quantities from Eq. (20), the governing Eq. (19) for a fracture with multiple power-law fluids can be rewritten in the dimensionless form as follows:

$$\begin{aligned}1 - \tilde{w} + \frac{8}{\pi}\int_0^\infty G\left(\frac{\tilde{s}}{\tilde{x}}\right)\Bigg(&\xi_1\left(1 + \frac{\chi}{\tilde{w}(\tilde{s})}\right)^{n_1}\frac{\tilde{s}^{1-n_1}}{\tilde{w}(\tilde{s})^{1+n_1}}\left(1 - H(\tilde{s} - \tilde{b}_1)\right) \\ &+ \sum_{i=2}^{N-1}\xi_i\left(1 + \frac{\chi}{\tilde{w}(\tilde{s})}\right)^{n_i}\frac{\tilde{s}^{1-n_i}}{\tilde{w}(\tilde{s})^{1+n_i}}\left(H(\tilde{s} - \tilde{b}_{i-1}) - H(\tilde{s} - \tilde{b}_i)\right) \\ &+ \xi_N\left(1 + \frac{\chi}{\tilde{w}(\tilde{s})}\right)^{n_N}\frac{\tilde{s}^{1-n_N}}{\tilde{w}(\tilde{s})^{1+n_N}}\left(H(\tilde{s} - \tilde{b}_{N-1})\right)\Bigg)\mathrm{d}\tilde{s} = 0\end{aligned} \tag{21}$$

where the kernel of the integral is of the form

$$G(t) = \frac{1 - t^2}{t}\ln\left|\frac{1 + t}{1 - t}\right| + 2 \tag{22}$$

As discussed by Dontsov and Peirce (2015b), this kernel is nonsingular. Next, the scaled governing Eq. (21) is discretized using Simpson's rule and is solved numerically using Newton's method for the parameters $n_1, n_2, \ldots, n_N$; χ; $\xi_1, \xi_2, \ldots, \xi_N$; and $b_1, b_2, \ldots, b_{N-1}$ to obtain fracture opening $\tilde{w}(\tilde{x})$. As an initial

guess, the maximum between limiting solutions for the first fluid is used. Explicit expressions for these asymptotic solutions for each fluid are provided next.

Asymptotic Solutions

This section presents toughness-, viscosity-, and leak-off-dominated asymptotic solutions for the ith fluid. The toughness-dominated solution is obtained from Eq. (19) in the limit of $M_i' = 0$, which gives the dry crack solution (Rice 1968)

$$w_k = \frac{K'}{E'} x^{1/2} \tag{23}$$

Viscous (m_i) and leak-off ($\tilde{m}_i$) limiting solutions for the particular fluid are obtained from Eq. (19) or its scaled analogue [Eq. (21)] by considering the region with this fluid, $(b_{i-1}, b_i]$ for the ith fluid, and assuming the dominance of either viscosity ($K' = 0$, $C' = 0$) or leak-off ($K' = 0$, $C' \to \infty$) term. Solution for the viscosity-dominated regime w_{m_i} is of the form

$$w_{m_i} = \left(\beta_{m_i} \frac{V^{n_i} M_i'}{E'}\right)^{1/(2+n_i)} x^{2/(2+n_i)}, \quad \text{with}$$
$$\beta_{m_i} = \frac{2(2+n_i)^2}{n_i} \tan\left(\frac{\pi n_i}{2+n_i}\right) \tag{24}$$

and for the leak-off-dominated regime $w_{\tilde{m}_i}$ is written

$$w_{\tilde{m}_i} = \left(\beta_{\tilde{m}_i} \frac{(2C')^{n_i} V^{n_i/2} M_i'}{E'}\right)^{1/(2(1+n_i))} x^{(4+n_i)/(4(1+n_i))},$$
$$\text{with} \quad \beta_{\tilde{m}_i} = \frac{64(1+n_i)^2}{3n_i(4+n_i)} \tan\left(\frac{3\pi n_i}{4(1+n_i)}\right) \tag{25}$$

For the particular case of $n_i = 0$, coefficients β are equal: $\beta_{\tilde{m}_i} = \beta_{m_i} = 4\pi$. Eqs. (24) and (25) correspond to the limiting solutions for the case of a single power-law fluid (Desroches et al. 1994; Lenoach 1995). However, the scaled form of the limiting solutions for the multifluid case differs from that for one power-law fluid due to the specifics of scaling used.

The limiting solutions [Eqs. (23)–(25)] are rewritten in terms of the scaled quantities [Eq. (20)] as follows:

$$\tilde{w}_k = 1, \tilde{w}_{m_i} = (\xi_i \beta_{m_i})^{1/(2+n_i)} \tilde{x}^{(2-n_i)/(2+n_i)},$$
$$\tilde{w}_{\tilde{m}_i} = (\xi_i \beta_{\tilde{m}_i})^{1/(2(1+n_i))} \chi^{n_i/(2(1+n_i))} \tilde{x}^{(2-n_i)/(2(1+n_i))} \tag{26}$$

The scaled viscosity and leak-off asymptotic solutions for each fluid in the multifluid case have an additional multiplier related to ξ_i compared with the case of a single fluid. This arises from the unified scaling used for all fluids used in this work.

For the case of identical fluids, which is equivalent to the case of a single fluid, it makes sense to choose the length scale parameter from Eq. (20) based on the properties of this fluid, $l = l_i$. In this case, one obtains $\xi_i = 1$ for all fluids and scaled limiting solutions [Eq. (26)] reduce to the corresponding solutions for one power-law fluid obtained by Gomez (2016) and Dontsov and Kresse (2018).

Numerical Results

The governing Eq. (21) is solved numerically to obtain scaled fracture opening $\tilde{w}$. The following dimensionless quantities are provided as the input parameters: leak-off coefficient χ, fluid properties ξ_i and n_i, and boundaries between fluids $\tilde{b}_i$. These quantities are obtained using Eqs. (4) and (20) from the prescribed parameters of the rock and fluids, as well as the fluid leak-off coefficient, fracture propagation velocity, and boundaries between the fluids. Most of the numerical results are demonstrated for the following parameters:

$$E = 20 \text{ GPa}, \quad \nu = 0.2, \quad K_{Ic} = 1 \text{ MPa} \cdot \text{m}^{0.5},$$
$$C_L = 10^{-4} \text{ m/s}^{0.5}, \quad V = 10^{-2} \text{m/s} \tag{27}$$

which determine the dimensionless leak-off coefficient as $\chi \approx 26$. The length scale l is estimated based on the properties of water ($k = 1$ mPa · s and $n = 1$) and other prescribed parameters [Eq. (27)] as $l \approx 3.9 \cdot 10^5$ m.

Next, estimates are provided to check applicability of the one-dimensional Carter's leak-off model for parameters in Eq. (27). The one-dimensional Carter's leak-off model is applicable as soon as the distance from the fracture tip much larger than the diffusion length scale

$$x \gg \sqrt{4Dt} \tag{28}$$

or equivalently

$$\sqrt{\frac{4D}{Vx}} \ll 1 \tag{29}$$

where D = diffusion coefficient in the reservoir; V = fracture propagation velocity; and x = typical distance from the tip. By focusing solely on the reservoir part of the leak-off coefficient, the Carter's coefficient can be estimated from (Economides and Nolte 2000)

$$C_L = \frac{\kappa(\sigma_0 - p_0)}{\mu\sqrt{\pi D}} \tag{30}$$

using the diffusion coefficient

$$D = \frac{\kappa M}{\mu} \tag{31}$$

where κ = permeability; and pore compressibility modulus M is given by

$$M = \left(\frac{\phi}{K_f} + \frac{1-\phi}{K_s}\right)^{-1} \tag{32}$$

where K_f and K_s = bulk moduli of fluid and solid; and ϕ = porosity of the rock. Estimate the magnitude of Carter's leak-off coefficient for the rock and fluid with the following properties: $K_f = 0.2$ GPa, $K_s = E/[3(1-2\nu)] \approx 11$ GPa, $\phi = 0.2$, $\mu = 1$ mPa · s, $\kappa = 0.3$ mDa (1 Da ≈ 1 μm^2), and $\sigma_0 - p_0 = 10$ MPa. Then, the leak-off coefficient can be estimated as $C_L \approx 1 \cdot 10^{-4}$ m/s$^{0.5}$. Using the propagation velocity of $V = 1$ cm/s and distance from the tip $x = 10$ m, the characteristic parameter in Eq. (29) becomes $\sqrt{4D/Vx} \approx 0.1$. Therefore, for the chosen parameters, the inequality Eq. (29) is satisfied for distances from the tip considered in this paper, and the applicability of Carter's leak-off model is justified. The diffusion length scale and Carter's coefficient are not directly correlated. That is, one can find a situation with relatively large value for the diffusion length scale and small C_L. At the same time, there are physically admissible situations, in which the diffusion length scale is small, whereas C_L is high.

Fracturing fluids can vary from low-viscosity solutions such as slick water (waterfrac) with a viscosity of the order of several mPa · s to more viscous gel-like fluids such as linear gels (viscosity of approximately 50 mPa · s) and higher-viscosity gel-like fluids with the addition of cross-linked polymers (viscosity of 100−1,000 mPa · s) (Montgomery 2013). The numerical results are demonstrated for the fluids rheologies provided in Table 1.

Table 1. Parameters of power-law fluids used in calculations

Fluid	Consistency index, k (10^{-3} Pa · s^n)	Flow index, n
Slick water	3	1
Linear gel 1	10	1
Linear gel 2	40	1
Cross-linked gel	1,436	0.58

Table 2. Modeling parameters used for different propagation regimes

Regime	E (GPa)	ν	K_{Ic} (MPa · m$^{0.5}$)	V (m/s)	C_L (m/s$^{0.5}$)	b_1 (m)
Toughness, k	5	0.2	2	10^{-3}	10^{-4}	0.5
Leak-off, $\tilde{m}$	20	0.2	1	10^{-2}	$5 \cdot 10^{-4}$	50
Viscosity, m	20	0.2	1	0.1	10^{-8}	50

The first three fluids are Newtonian with the viscosity 3, 10, and 40 mPa · s, whereas the last fluid is power-law fluid with the consistency index $k = 1.436$ Pa · s^n and flow index $n = 0.58$. The boundaries between the fluids b_i were varied from 0.5 to 50 m for most of the results. To investigate the solution's behavior in different propagation regimes, this study considered the fracture with two fluids (slick water and linear gel 1) for the parameters provided in Table 2. For the cases where the propagation regime is not specified, parameters in Eq. (27) are used.

Comparison between One-Fluid and Two-Fluids Solutions

This section presents the numerical solution for the scaled fracture opening $\tilde{w}(\tilde{x})$ for the case of two fluids: slick water followed by cross-linked gel from Table 1. It is important to mention that the scaled fracture opening $\tilde{w}$ is related to the apparent fracture toughness; it is equal to 1 at the fracture tip and increases with distance from the tip. The numerical results are shown on a logarithmic scale to illustrate the solution at different length scales. For the case of two fluids, one boundary between them, b_1, is specified. The solutions for various boundary locations were obtained: $b_1 = 0.5$ m and $b_1 = 50$ m, which corresponds to smaller and larger volume of the first injected fluid, respectively. Other parameters used are given in Eq. (27).

Fig. 2 shows the multifluid numerical solutions (solid lines) with the varied location of the boundary between fluids shown by gray vertical lines. For comparison, the one-fluid solution for slick water is shown by the dashed line and the one for a cross-linked gel by the other dashed line. Solutions for each fluid have different slopes far from the tip because they are determined by the flow index n (which is different) and the propagation regime according to Eq. (26).

For the presented case, the first fluid is Newtonian with the flow index $n = 1$, whereas the second fluid is power-law with the flow index $n = 0.58$; therefore, the slope is steeper for the second fluid. This behavior means that, given that a hydraulic fracture propagates with the same velocity, the apparent fracture toughness is larger for a power-law fluid than for a Newtonian fluid. Also, the intercept of $\tilde{w}$ on a logarithmic scale depends on both flow index n and consistency index k as well as the propagation regime according to Eq. (26). The limiting solutions are not plotted in Fig. 2; however, $b_1 = 0.5$ m corresponds to the toughness–leak-off transition and $b_1 = 50$ m is very close to the viscosity propagation regime for both fluids.

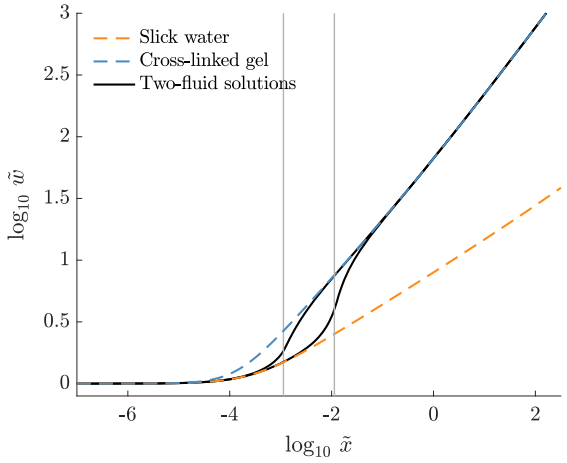

Fig. 2. Numerical solution for a semi-infinite HF with a single fluid (slick water and cross-linked gel) and with two fluids for different locations of the boundary between fluids shown by vertical lines: $b_1 = 0.5$ m and $b_1 = 50$ m.

The multifluid solution asymptotically reaches the solution for the first fluid near the fracture tip (before the boundary) and the solution for the second fluid far from the tip (after the boundary), which can be observed on a logarithmic scale. In between, the solution smoothly transitions between them. The transition region extends far beyond the location of the boundary between fluids due to the nonlocal effect of the integral kernel in the elasticity relation. The transition behavior depends on both the location of the boundary between the fluids and fluid properties contrast, assuming all other parameters of a propagating fracture are the same. The transition occurs closer to the tip at the boundary location $b_1 = 0.5$ m compared with $b_1 = 50$ m. The aforementioned asymptotic behavior can be generalized for any number of sequential fluids as follows: the numerical solution for multiple fluids asymptotically approaches the solution for the first fluid near the fracture tip and the solution for the last fluid far away from the tip. From a practical perspective, the nonlocality of the response means that the injection of a high-viscosity fluid at the end of the treatment may significantly alter fracture behavior at distances further away from the boundary between the fluids.

Analysis of the Solution with Respect to Propagation Regime

To investigate the solution for two fluids in different propagation regimes, the problem parameters were specified so that the boundary between the fluids falls into the length scale of the corresponding propagation regime for both fluids. The parameters used for toughness, viscosity, and leak-off dominated regimes are provided in Table 2. To focus purely on the effects of fluid viscosity and exclude the solution's dependence on the flow index, two Newtonian fluids with different viscosities are considered: slick water and linear gel 1 from Table 1.

For the toughness-dominated regime, Fig. 3 shows the scaled fracture opening for a different order of fluids: Fig. 3(a) shows a less viscous fluid (slick water) followed by a more viscous fluid (linear gel), and Fig. 3(b) shows a more viscous fluid followed by a less viscous fluid. In both plots, the solution for the slick water is shown by the dashed lines and the one for the linear gel is shown by the other dashed lines. The solid line corresponds to the multifluid solution with the boundary between fluids (gray vertical line)

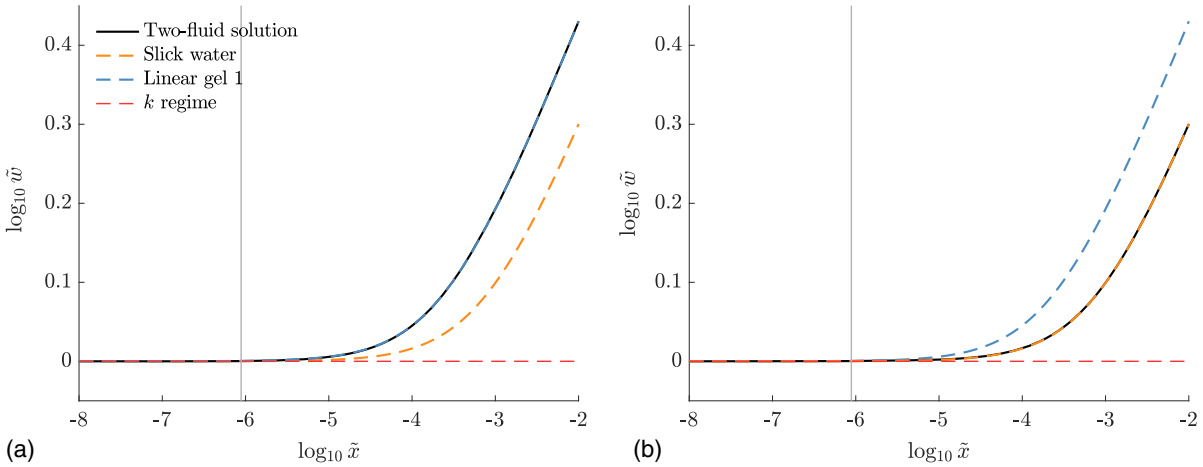

Fig. 3. Numerical solution for two different Newtonian fluids with the boundary located in the toughness-dominated regime: (a) less viscous slick water followed by a more viscous linear gel 1; and (b) the opposite order.

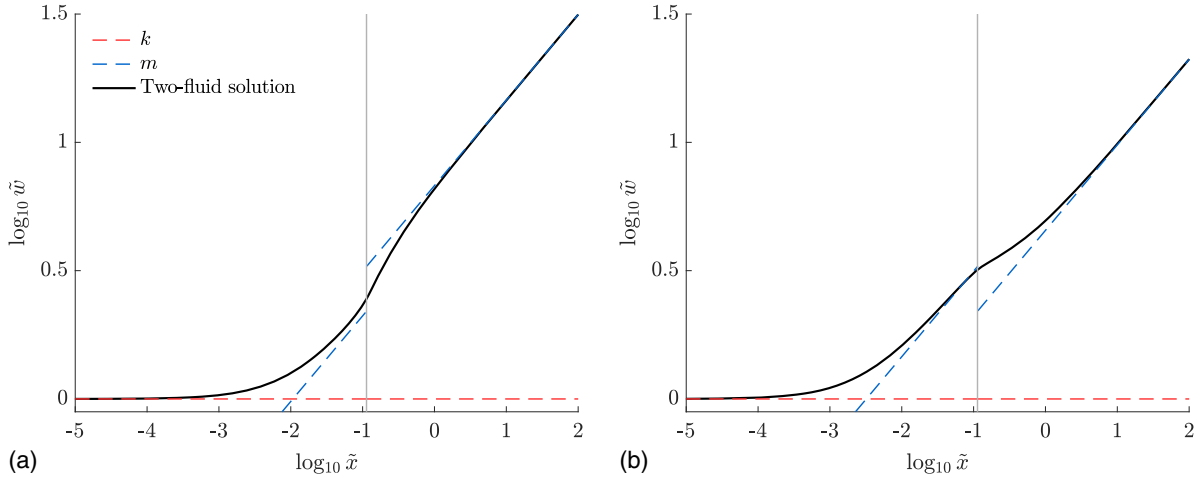

Fig. 4. Numerical solution for two different Newtonian fluids with the boundary located in the viscosity-dominated regime: (a) less viscous slick water followed by a more viscous linear gel 1; and (b) the opposite order.

located within the toughness-dominated regime. The limiting solution for the toughness-dominated regime $\tilde{w} = 1$ corresponds to the solution for a dry fracture and is shown by a horizontal line. The solution for any hydraulic fracture asymptotically approaches this solution for a dry fracture at a small length scale near the fracture tip.

For the multifluid solution, the transition from the solution for the first fluid to the solution for the second fluid (for any fluid order) is not visible because it effectively occurs between the toughness asymptotes that are the same for both fluids. As a result, as expected, the multifluid solution coincides with the solution for the second fluid [linear gel in Fig. 3(a) and slick water in Fig. 3(b)] throughout the whole fracture. Also, due to a larger viscosity of the linear gel, it provides a larger increase in the apparent fracture toughness than slick water.

For the case when the boundary between fluids is located in the viscosity-dominated regime, the solution is provided in Fig. 4 in the same form as in Fig. 3 except that the viscosity-dominated asymptotes (m, dashed lines) are plotted instead of full solutions for slick water and linear gel. The dashed line before the boundary corresponds to the viscous asymptote of the first fluid, and the one after the boundary corresponds to the viscous asymptote of the second fluid. For the considered case of two Newtonian fluids, these asymptotes have the same slope (because $n_1 = n_2$) and different intercepts (because $k_1 \neq k_2$). The intercept of the asymptote is larger for the fluid with the larger consistency index k, i.e., for the second fluid in Fig. 4(a) and for the first fluid in Fig. 4(b).

Because the boundary between fluids is located in the viscosity-dominated regime for both fluids, the multifluid solution (solid line) transitions between corresponding viscous asymptotic solutions of these fluids. For the case of less viscous slick water followed by a more viscous linear gel [Fig. 4(a)], the solution transitions from the lower asymptote to the higher asymptote by accelerating the increase of the scaled fracture opening. For the opposite case of more viscous fluid followed by a less viscous fluid [Fig. 4(b)], the transition occurs from the higher asymptote to the lower one. However, in this case, the fracture opening does not immediately decrease to follow the lower asymptote; instead, it slightly slows down the width growth until it meets the asymptote. The scenario of more viscous fluid followed by a less viscous fluid corresponds to the unstable flow solution, but it is included for completeness.

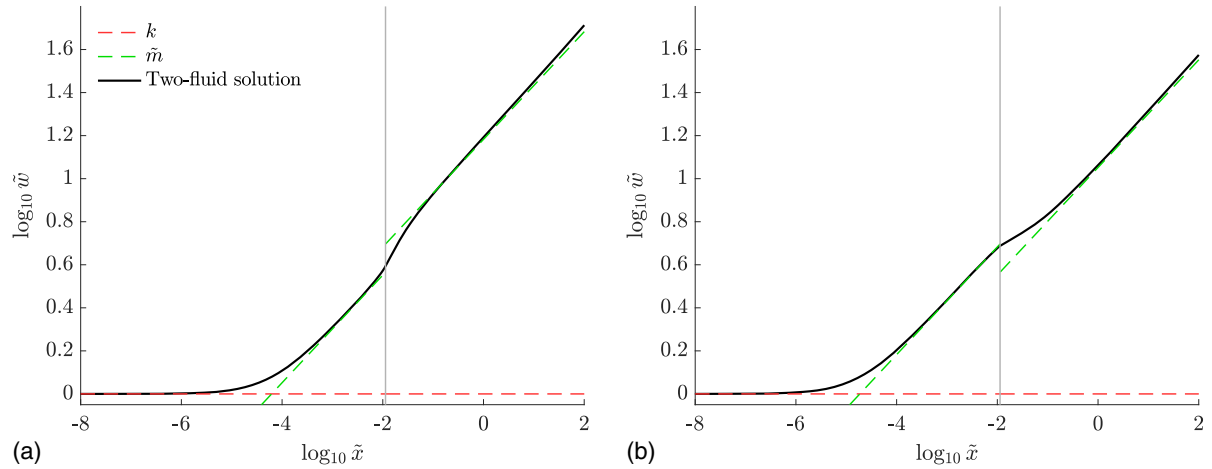

Fig. 5. Numerical solution for two different Newtonian fluids with the boundary located in the leak-off-dominated regime: (a) less viscous slick water followed by a more viscous linear gel 1; and (b) the opposite order.

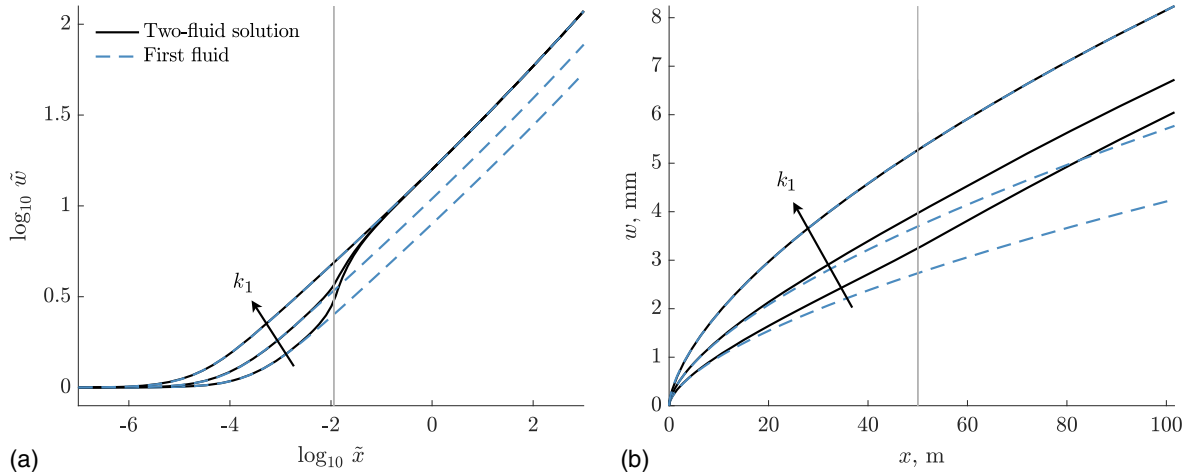

Fig. 6. Sensitivity of (a) scaled; and (b) unscaled fracture opening of the HF with two fluids to the consistency index of the first fluid $k_1 = 3, 10, 40\,\text{mPa} \cdot \text{s}$ at $k_2 = 40\ \text{mPa} \cdot \text{s}$.

For the leak-off-dominated regime, the solution is shown in Fig. 5 in the same form as in Fig. 4. In this case, the transition between fluids occurs from the leak-off-dominated asymptote of the first fluid (line before the boundary) to the one of the second fluid (line after the boundary). Also, the leak-off-dominated case corresponds to the higher apparent fracture toughness. Otherwise, the behavior of the solutions is qualitatively the same as for the viscosity-dominated case (Fig. 4).

Effect of Viscosity Contrast for Two Newtonian Fluids

This section investigates the sensitivity of the numerical solution to the viscosity of one of the two Newtonian fluids in a fracture. The fluid viscosity was varied in a range from 3 to 40 mPa · s, and other parameters used are specified in Eq. (27).

To illustrate the case of a lower-viscosity fluid followed by a higher-viscosity fluid, Fig. 6 shows sensitivity of the solution to the viscosity of the first fluid $k_1 = 3, 10, 40\,\text{mPa} \cdot \text{s}$ for the fixed viscosity of the second fluid $k_2 = 40\,\text{mPa} \cdot \text{s}$. Solid lines show the numerical solution in the presence of both fluids, and the dashed lines show the one-fluid solutions corresponding to the first fluid. Fig. 6(a) shows the solution $\tilde{w}$ in the scaled form, and Fig. 6(b) shows the fracture opening w in millimeters versus physical distance from the tip x in meters.

On a logarithmic scale, all solutions asymptotically reach the solution for the second fluid with $k = 40\,\text{mPa} \cdot \text{s}$ far away from the tip. At the same time, in the shown range of values of x up to 100 m, the transition to this asymptote does not occur. Instead, the solution in this range is determined by the transition zone right near the boundary, which is of great interest for hydraulic fracturing applications. The solution in the transition zone depends on the contrast of fluid properties. The increase of the viscosity of the first fluid shifts the corresponding solution upward by increasing the apparent fracture toughness and fracture opening, given that other parameters are the same.

Fig. 7 shows the sensitivity of the solution to the viscosity of the second fluid, focusing on the case of a lower-viscosity fluid with $k_1 = 3\,\text{mPa} \cdot \text{s}$ followed by a higher-viscosity fluid $k_2 = 3, 10, 40\,\text{mPa} \cdot \text{s}$. The solid lines show the two-fluid solution, as before, but dashed lines here correspond to the solution for the second fluid. In this case, all multifluid solutions show similar behavior near the fracture tip by following the asymptote for the fluid with $k = 3\,\text{mPa} \cdot \text{s}$. On a logarithmic scale [Fig. 7(a)], multifluid solutions asymptotically reach the corresponding solutions for the second fluid

J. Eng. Mech., 2021, 147(10): 04021064

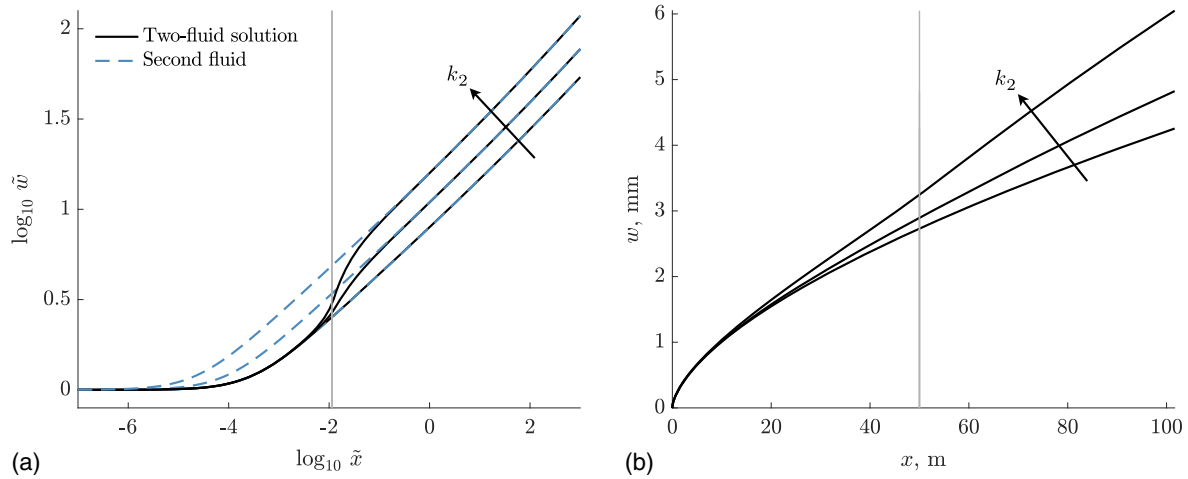

Fig. 7. Sensitivity of (a) scaled; and (b) unscaled fracture opening of the HF with two fluids to the consistency index of the second fluid $k_2 = 3, 10, 40\,\text{mPa} \cdot \text{s}$ at $k_1 = 3\ \text{mPa} \cdot \text{s}$.

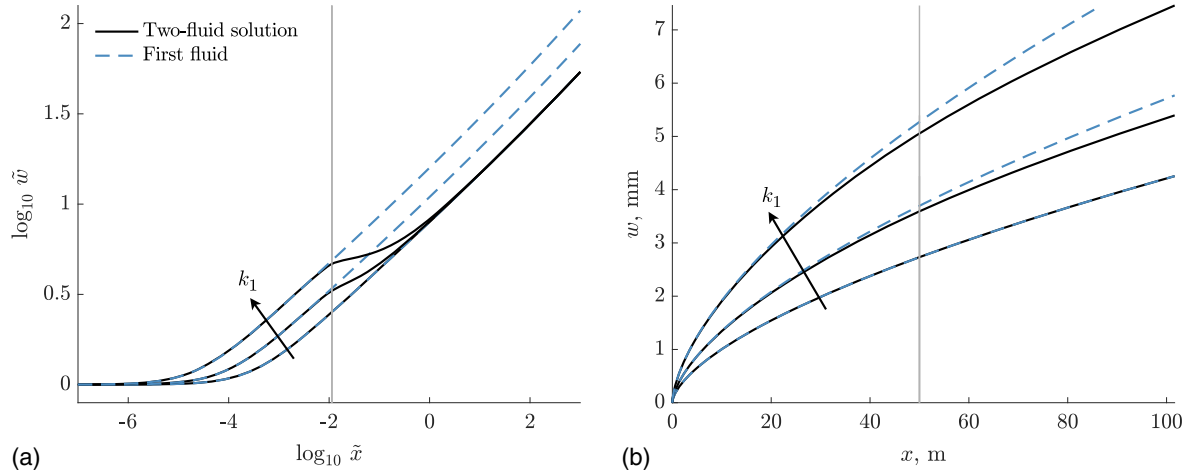

Fig. 8. Sensitivity of (a) scaled; and (b) unscaled fracture opening of the HF with two fluids to the consistency index of the first fluid $k_1 = 3, 10, 40\ \text{mPa} \cdot \text{s}$ at $k_2 = 3\ \text{mPa} \cdot \text{s}$.

far away from the tip. However, this is not observed for the considered range of $x = [0, 100]$ m; therefore, the solutions for the second fluid are not shown in Fig. 7(b). Again, the solution in the physical range of x mostly reflects the transition zone that spans not only behind the boundary but also to some region in front of it. The larger the contrast of properties between the first and the second fluid, the larger the increase of the apparent fracture toughness and the fracture opening represented by the transition to the higher-viscosity solution.

Next, similar numerical results are shown for the case of a higher-viscosity fluid followed by a lower-viscosity fluid. In this scenario, the instabilities on the boundaries between fluids may develop, which may restrict the applicability of the developed model. However, the instabilities usually require some time to develop and to reach the scale at which they become relevant. For each particular case, estimation of the effects of instabilities may be required. For completeness, the results of the model are provided assuming that instabilities are not relevant for the analysis. Fig. 8 shows the results for the sensitivity to the viscosity of the first fluid $k_1 = 3, 10, 40\,\text{mPa} \cdot \text{s}$ at $k_2 = 3\,\text{mPa} \cdot \text{s}$, and Fig. 9 shows the results for varied viscosity of the second fluid $k_2 = 3, 10, 40\ \text{mPa} \cdot \text{s}$ at $k_1 = 40\ \text{mPa} \cdot \text{s}$.

In these cases, the transition occurs from the solution for the more viscous fluid to the solution for the lower-viscosity fluid. The larger the contrast of properties, the wider the transition zone. For the high contrast of fluid properties, $\tilde{w}$ in the transition zone behind the boundary almost reaches the plateau. The exact plateau ($\tilde{w} = \text{constant}$) would mean that in this region the apparent fracture toughness K_{app} is constant, and the shape of the fracture opening is close to the square-root behavior $w \propto x^{1/2}$ as for a dry crack but with the increased fracture toughness $K_{\text{app}} = \text{constant} \times K_{Ic}$.

Newtonian Fluid Followed by Power-Law Fluid

This section compares the multifluid solution for a Newtonian fluid and a power-law fluid depending on the fluid order. As an example, the following fluids are considered: slick water and cross-linked gel from Table 1 that represent the Newtonian and power-law fluids, respectively. It is assumed that the boundary between the fluids is located at a distance from the fracture tip $b = 10$ m.

Fig. 10 shows the scaled [Fig. 10(a)] and unscaled [Fig. 10(b)] fracture opening for a fracture with Newtonian fluid followed by power-law fluid (solid line, see label) and with the opposite

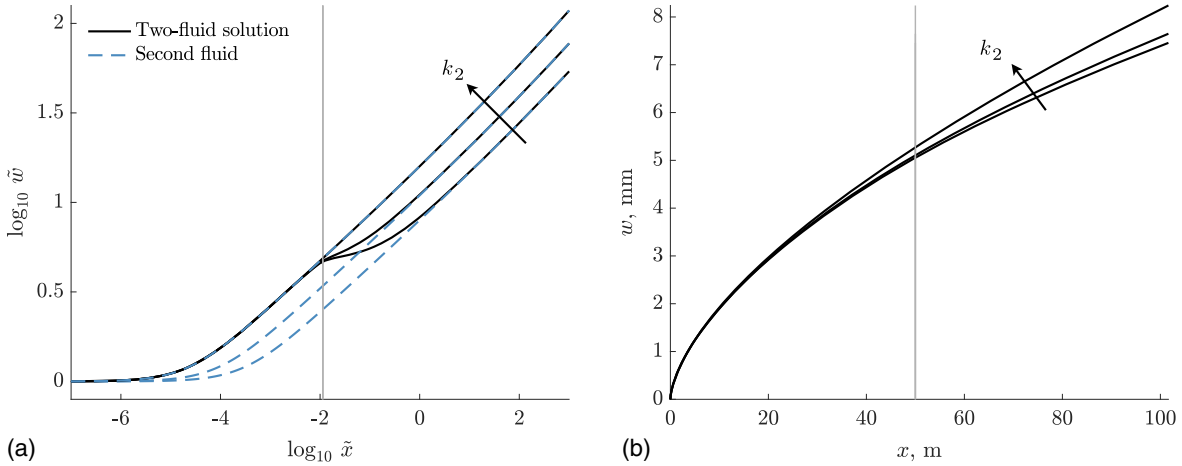

Fig. 9. Sensitivity of (a) scaled; and (b) unscaled fracture opening of the HF with two fluids to the consistency index of the second fluid $k_2 = 3, 10, 40$ mPa · s at $k_1 = 40$ mPa · s.

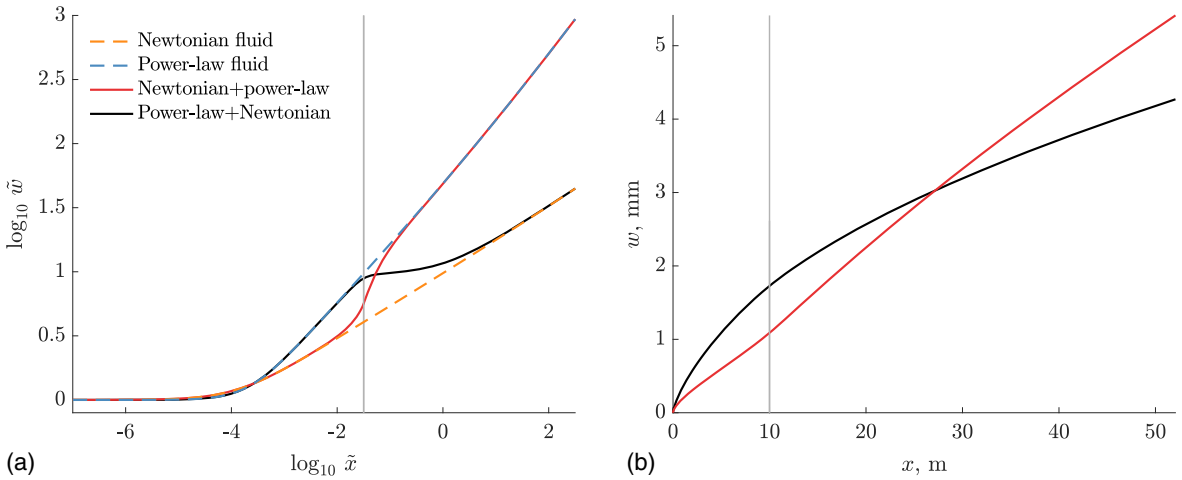

Fig. 10. Sensitivity of (a) scaled; and (b) unscaled fracture opening of the HF with two fluids, Newtonian fluid and power-law fluid, injected in different order.

order of fluids (another solid line, see label). As previously discussed, the transition between the one-fluid solutions for a Newtonian fluid (dashed line, see label) and a power-law fluid (another dashed line, see label) occurs, or the opposite depending on the fluid order. In this case, the one-fluid solutions have different slopes on a logarithmic scale, which are determined by the flow indices $n = 1$ and $n = 0.58$ of the considered fluids.

For the Newtonian fluid followed by power-law fluid, the transition occurs to the solution with a larger $\tilde{w}$. However, for the power-law fluid followed by the Newtonian fluid, the close to plateau behavior of $\tilde{w}$ is observed in a transition region. The latter behavior corresponds to the toughness-dominated solution with some value of apparent toughness, which is similar to the case of more viscous fluid followed by a less viscous fluid, described previously. In case of displacement of a more viscous fluid by a less viscous fluid, the use of the current model may be limited due to possible instabilities that may develop on the fluid–fluid interface that are not considered by the model. Similar limitations can relate to the considered case of a power-law fluid followed by a Newtonian fluid.

In spite of that, it is interesting to investigate how fracture opening depends on the fluid order. The apparent fracture toughness before the fluid boundary is larger when the first fluid is power-law. Behind the boundary, there is a transition zone where this trend stays, but farther, there is an intersection point behind which the apparent fracture toughness with Newtonian fluid injected first becomes larger. This is consistent with the fact that the considered power-law fluid provides a larger increase in a fracture toughness felt by a crack compared with the Newtonian fluid. The same result can be concluded for the fracture opening assuming the same fracture propagation velocities. However, because in reality the velocities are different, a fracture opening needs to be recalculated accordingly.

Solution for Three Fluids

This section shows the solution for a semi-infinite HF with three sequentially injected fluids. In this case, the locations of two boundaries b_1 and b_2 are specified. As an example, three Newtonian fluids from Table 1 are considered in the following order: slick water followed by linear gel 1 followed by linear gel 2. This scenario corresponds to the fluids injected in the order of increasing

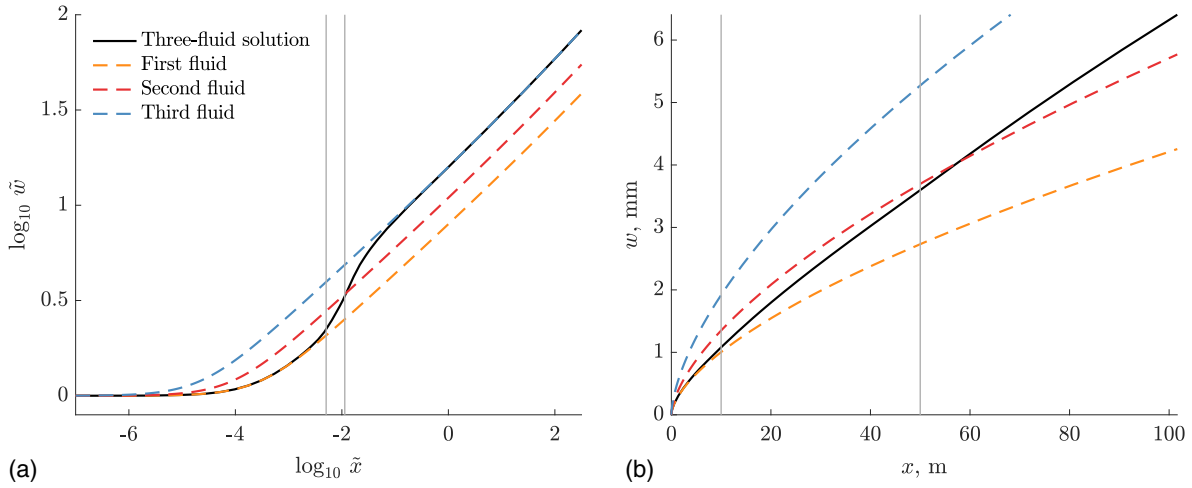

Fig. 11. (a) Scaled; and (b) unscaled solutions for the case of three fluids.

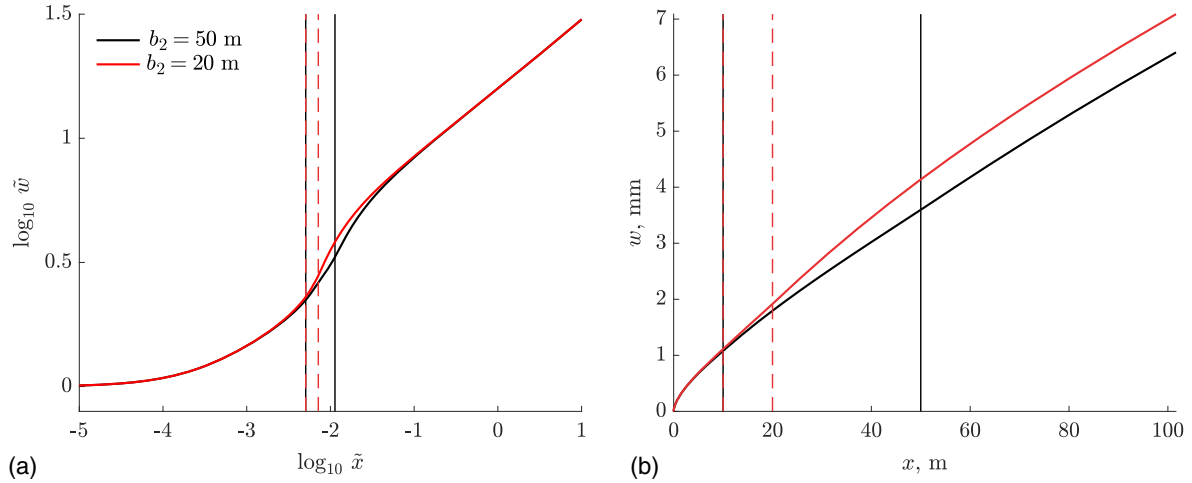

Fig. 12. (a) Scaled; and (b) unscaled solutions for the case of three fluids with smaller and larger region occupied by the intermediate fluid. Vertical lines show the boundaries between fluids for the solution.

viscosity (3, 10, and 40 mPa · s). Other parameters used are given in Eq. (27).

Fig. 11 shows the numerical solution (solid lines) for the boundaries between fluids $b_1 = 10$ m and $b_2 = 50$ m (gray lines). The solutions for the first, second, and third fluids are shown by the other lines. Near the tip, the multifluid solution follows the solution for the first fluid, whereas far away from the tip, it follows the solution for the third fluid. The intermediate fluid asymptote is not reached even on a logarithmic scale.

To compare the multifluid numerical solutions for the different lengths of the region occupied by the intermediate fluid, the location of the second boundary is changed from $b_2 = 50$ m to $b_2 = 20$ m. Fig. 12 shows the corresponding multifluid solutions. The boundaries are shown by vertical lines. The shift of the boundary significantly changes the fracture opening, i.e., the length of the region with the intermediate fluid affects the solution even though its asymptote is not reached. Specifically, in the considered case, the larger region with the intermediate fluid delays the transition to the one-fluid solution of the last fluid (one-fluid solutions are shown in Fig. 11), making effective fracture toughness (and fracture opening) in the transition region smaller.

Summary

The problem of a semi-infinite hydraulic fracture propagating with multiple immiscible sequentially injected power-law fluids was solved numerically. The solution for the fracture opening asymptotically approaches the solution for the first fluid near the fracture tip and the solution for the last fluid far away from the tip. The behavior in a transition region also depends on the properties of the intermediate fluids (if any) and the location of the boundaries between them. However, the corresponding limiting solutions of the intermediate fluids cannot always be reached in practice. The transition region is located near the boundary and, even in the assumption of a localized jump of fluid properties on the boundary, this region spans far beyond the boundary location due to the nonlocal effect associated with elastic interactions. The transition zone between fluids increases in size with increasing contrast of the fluid properties. This nonlocal response leads to the fact that the injection of a high-viscosity fluid toward the end of the treatment, which is commonly the case in practice, may significantly alter fracture behavior ahead of the fluid interface and can even temporarily arrest further fracture propagation.

For the case of two fluids, depending on problem parameters, the numerical solution captures the limiting solutions corresponding to different propagation regimes related to each fluid. For the interface between fluids located in different propagation regimes, the transition between the corresponding asymptotic solutions was demonstrated. For the transition in the toughness-dominated regime, the two-fluid solution is equivalent to the solution for the second fluid. For the viscosity-dominated regime, the transition from the viscous asymptote of the first fluid to the one of the second fluid occurs. The difference between the asymptotic solutions is determined by different flow and consistency indices of the fluids. Fluids with larger viscosity (or consistency index) cause a larger increase of the apparent fracture toughness. A similar transition occurs for the leak-off-dominated regime.

In the particular case of two Newtonian fluids with a specified location of the interface, the transition is determined by the contrast of fluid viscosities. Higher viscosity corresponds to a larger fracture opening under the condition of a constant velocity of fracture propagation. The fluid order determines the fracture shape. The solutions corresponding to different orders of the same fluids intersect at a point behind the boundary. Similar behavior was demonstrated on the example of two fluids with different rheologies: Newtonian and power-law. In this case, different flow and consistency indices determine the transition between the corresponding one-fluid solutions. It is worth reiterating that in the long term, the resistance to fracture growth is determined by the properties of the last fluid. In practical cases, however, this situation may not always be reached, and hence the behavior is affected by all fluids that are present in the fracture.

For more than two fluids, the asymptotic solutions for the intermediate fluids are not reached in practice due to the nonlocal effect of elasticity. However, it was showed that the presence of intermediate fluids significantly alters the solution in the transition zone; therefore, it must be considered. Asymptotic solutions for multiple power-law fluids were implemented in a commercial HF simulator (Dontsov et al. 2019) to track the fracture front for the cases when multiple fracturing fluids are used in the treatment.

Data Availability Statement

The computer code developed in this study is available from the corresponding author by request.

Acknowledgments

The initial results of this work were obtained during the internship of the first author at W. D. Von Gonten laboratories. Permission to publish is greatly acknowledged.

References

Adachi, J. I. 2001. *Fluid-driven fracture in permeable rock*. Minneapolis: Univ. of Minnesota.

Al-Housseiny, T. T., P. A. Tsai, and H. A. Stone. 2012. "Control of interfacial instabilities using flow geometry." *Nat. Phys.* 8 (10): 747–750. https://doi.org/10.1038/nphys2396.

Barbati, A. C., J. Desroches, A. Robisson, and G. H. McKinley. 2016. "Complex fluids and hydraulic fracturing." *Annu. Rev. Chem. Biomol. Eng.* 7 (1): 415–453. https://doi.org/10.1146/annurev-chembioeng-080615-033630.

Belyadi, H., E. Fathi, and F. Belyadi. 2016. *Hydraulic fracturing in unconventional reservoirs: Theories, operations, and economic analysis*. Houston: Gulf Publishing.

Bessmertnykh, A. O., and E. V. Dontsov. 2018. "Aspect ratio of hydraulic fracture in homogeneous transversely isotropic material." In *Proc., 52nd US Rock Mechanics/Geomechanics Symp.* Alexandria, VA: American Rock Mechanics Association.

Bessmertnykh, A. O., and E. V. Dontsov. 2019. "A semi-infinite hydraulic fracture driven by a Herschel-Bulkley fluid." *J. Appl. Mech.* 86 (12): 121008. https://doi.org/10.1115/1.4044815.

Carter, E. 1957. "Optimum fluid characteristics for fracture extension." In *Drilling and production practice*, edited by G. C. Howard and C. R. Fast, 261–270. College Park, MD: American Institute of Physics.

Desroches, J., E. Detournay, B. Lenoach, P. Papanastasiou, J. Pearson, M. Thiercelin, and A.-D. Cheng. 1994. "The crack tip region in hydraulic fracturing." *Proc. R. Soc. London, Ser. A* 447 (1929): 39–48. https://doi.org/10.1098/rspa.1994.0127.

Detournay, E. 2016. "Mechanics of hydraulic fractures." *Annu. Rev. Fluid Mech.* 48 (1): 311–339. https://doi.org/10.1146/annurev-fluid-010814-014736.

Dontsov, E. 2017. "An approximate solution for a plane strain hydraulic fracture that accounts for fracture toughness, fluid viscosity, and leak-off." *Int. J. Fract.* 205 (2): 221–237. https://doi.org/10.1007/s10704-017-0192-4.

Dontsov, E., A. Bunger, B. Abell, and R. Suarez-Rivera. 2019. "Ultrafast hydraulic fracturing model for optimizing cube development." In *Proc., Unconventional Resources Technology Conf.* Tulsa, OK: Society of Exploration Geophysicists.

Dontsov, E. V. 2016. "An approximate solution for a penny-shaped hydraulic fracture that accounts for fracture toughness, fluid viscosity and leak-off." *R. Soc. Open Sci.* 3 (12): 160737. https://doi.org/10.1098/rsos.160737.

Dontsov, E. V. 2019. "Scaling laws for hydraulic fractures driven by a power-law fluid in homogeneous anisotropic rocks." *Int. J. Numer. Anal. Methods Geomech.* 43 (2): 519–529. https://doi.org/10.1002/nag.2874.

Dontsov, E. V., and O. Kresse. 2018. "A semi-infinite hydraulic fracture with leak-off driven by a power-law fluid." *J. Fluid Mech.* 837: 210–229. https://doi.org/10.1017/jfm.2017.856.

Dontsov, E. V., and A. P. Peirce. 2015a. "A Lagrangian approach to modelling proppant transport with tip screen-out in KGD hydraulic fractures." *Rock Mech. Rock Eng.* 48 (6): 2541–2550. https://doi.org/10.1007/s00603-015-0835-6.

Dontsov, E. V., and A. P. Peirce. 2015b. "A non-singular integral equation formulation to analyze multiscale behaviour in semi-infinite hydraulic fractures." *J. Fluid Mech.* 781: R1. https://doi.org/10.1017/jfm.2015.451.

Dontsov, E. V., and A. P. Peirce. 2017. "A multiscale implicit level set algorithm (ILSA) to model hydraulic fracture propagation incorporating combined viscous, toughness, and leak-off asymptotics." *Comput. Method Appl. Mech. Eng.* 313 (Jan): 53–84. https://doi.org/10.1016/j.cma.2016.09.017.

Economides, M. J., and K. G. Nolte. 2000. *Reservoir stimulation*. 3rd ed. Chichester, UK: Wiley.

Garagash, D. I., E. Detournay, and J. I. Adachi. 2011. "Multiscale tip asymptotics in hydraulic fracture with leak-off." *J. Fluid Mech.* 669: 260–297. https://doi.org/10.1017/S002211201000501X.

Gomez, D. 2016. "A non-singular integral equation formulation of permeable semi-infinite hydraulic fractures driven by shear-thinning fluids." M.S. thesis, Dept. of Mathematics, Univ. of British Columbia.

Gordeliy, E., and A. Peirce. 2013. "Implicit level set schemes for modeling hydraulic fractures using the XFEM." *Comput. Methods Appl. Mech. Eng.* 266: 125–143. https://doi.org/10.1016/j.cma.2013.07.016.

Lakhtychkin, A., D. Eskin, and O. Vinogradov. 2012. "Modelling of transport of two proppant-laden immiscible power-law fluids through an expanding fracture." *Can. J. Chem. Eng.* 90 (3): 528–543. https://doi.org/10.1002/cjce.20694.

Lakhtychkin, A., O. Vinogradov, and D. Eskin. 2011. "Modeling of placement of immiscible fluids of different rheology into a hydraulic fracture." *Ind. Eng. Chem. Res.* 50 (9): 5774–5782. https://doi.org/10.1021/ie101914d.

Lecampion, B., et al. 2013. "The impact of the near-tip logic on the accuracy and convergence rate of hydraulic fracture simulators compared to reference solutions." Chap. 43 in *Effective and sustainable hydraulic*

fracturing, edited by R. J. A. P. Bunger and J. McLennan, 855–873. Lisbon, Portugal: International Society for Rock Mechanics.
Lenoach, B. 1995. "The crack tip solution for hydraulic fracturing in a permeable solid." *J. Mech. Phys. Solids* 43 (7): 1025–1043. https://doi.org/10.1016/0022-5096(95)00026-F.
Montgomery, C. 2013. "Fracturing fluids." In *Effective and sustainable hydraulic fracturing*, edited by A. P. Bunger, J. McLennan, and R. Jeffrey. Rijeka, Croatia: International Society for Rock Mechanics and Rock Engineering.
Moukhtari, F.-E., B. Lecampion, and H. Zia. 2020. "Planar hydraulic fracture growth perpendicular to the isotropy plane in a transversely isotropic material." *J. Mech. Phys. Solids* 137 (Apr): 103878. https://doi.org/10.1016/j.jmps.2020.103878.
Peirce, A. 2016. "Implicit level set algorithms for modelling hydraulic fracture propagation." *Philos. Trans. R. Soc. London, Ser. A* 374 (2078): 20150423. https://doi.org/10.1098/rsta.2015.0423.
Peirce, A., and E. Detournay. 2008. "An implicit level set method for modeling hydraulically driven fractures." *Comput. Methods Appl. Mech. Eng.* 197 (33–40): 2858–2885. https://doi.org/10.1016/j.cma.2008.01.013.
Peshcherenko, A., and D. Chuprakov. 2021. "An ultrafast simulator for 3D propagation of a hydraulic fracture with rectangular shape." *Eng. Fract. Mech.* 243 (Feb): 107512. https://doi.org/10.1016/j.engfracmech.2020.107512.
Rice, J. R. 1968. "A path independent integral and the approximate analysis of strain concentration by notches and cracks." *J. Appl. Mech.* 35 (2): 379–386. https://doi.org/10.1115/1.3601206.
Roper, S. M., and J. R. Lister. 2007. "Buoyancy-driven crack propagation: The limit of large fracture toughness." *J. Fluid Mech.* 580: 359–380. https://doi.org/10.1017/S0022112007005472.
Saffman, P. G., and G. I. Taylor. 1958. "The penetration of a fluid into a porous medium or Hele-Shaw cell containing a more viscous liquid." *Proc. R. Soc. London, Ser. A* 245 (1242): 312–329. https://doi.org/10.1098/rspa.1958.0085.
Spence, D. A., P. W. Sharp, and D. L. Turcotte. 1987. "Buoyancy-driven crack propagation: A mechanism for magma migration." *J. Fluid Mech.* 174: 135–153. https://doi.org/10.1017/S0022112087000077.
Truzzolillo, D., and L. Cipelletti. 2017. "Hydrodynamic instabilities in miscible fluids." *J. Phys.: Condens. Matter* 30 (3): 033001.
Woods, A. W., and N. Mingotti. 2016. "Topographic viscous fingering: Fluid–fluid displacement in a channel of non-uniform gap width." *Philos. Trans. R. Soc. London, Ser. A* 374 (2078): 20150427. https://doi.org/10.1098/rsta.2015.0427.